Decision Analytics Journal 6 (2023) 100147

Contents lists available at ScienceDirect

Decision Analytics Journal

journal homepage: www.elsevier.com/locate/dajour

Design and evaluation of hysteresis models for structural systems using a fuzzy adaptive charged system search

Nima Mohajer Rahbari [a], Hedayat Veladi [b], Mahdi Azizi [b], Pooya Sareh [c,*], Siamak Talatahari [b,d]

[a] Department of Civil and Environmental Engineering, University of Alberta, Edmonton, Canada
[b] Department of Civil Engineering, University of Tabriz, Tabriz, Iran
[c] Creative Design Engineering Lab (Cdel), School of Engineering, University of Liverpool, Liverpool, L69 3GH, United Kingdom
[d] Faculty of Engineering & IT, University of Technology Sydney, Ultimo, NSW 2007, Australia

ARTICLE INFO

Keywords:
Hysteresis model
Nonlinear behavior
Bouc–Wen–Baber–Noori model
Parametric identification
Fuzzy adaptive charged system search

ABSTRACT

Many hysteresis models have been proposed for the simulation of the nonlinear behavior of structures each of which has certain advantages depending on specific applications and desired objectives. The Bouc–Wen–Baber–Noori model is one of the hysteresis models that has been utilized for a wide range of applications. However, the parameter tuning of this model has been conducted based on expert knowledge, which has not led to the development of a precise nonlinear model. The main contribution of this paper is to propose a metaheuristic-based parametric identification process for the design of the Bouc–Wen–Baber–Noori hysteresis model and evaluate the results by using some established experimental investigation methods. To fulfill this aim, the Fuzzy Adaptive Charged System Search (F-CSS) is proposed for optimization in which a fuzzy-logic-based parameter tuning process is utilized to achieve better performance in comparison with the standard Charged System Search algorithm (CSS). For nonlinear dynamic analysis, an Iterative Hysteretic Analysis (IHA) process is also introduced for conducting the precise analysis of the structure with exact solutions. Comparing the metaheuristic-based results to the experimental findings demonstrates that the proposed algorithm is capable of providing very competitive results. Besides, the proposed adaptive method is capable of producing very competitive results in comparison with different optimization algorithms.

1. Introduction

Hysteresis is an intricate memory-dependent nonlinear behavior in which the output of a system not only depends on the instantaneous input, but also on the past time-history of the input disturbances. This type of inelastic behavior is commonly observed in structural components such as reinforced concrete, steel, and wood elements. Other examples include base isolators, dampers, and soil profiles in which there is a nonlinear mechanism to supply the restoring force against external excitations and dissipate the input energy.

Devising a valid model for simulating the nonlinear hysteretic behavior of structural systems and integrating them into design methods has been always an ever-increasing challenge in the design of structures to withstand natural cyclic loads such as earthquakes and strong winds. In fact, major structures (e.g. bridges, towers, and industrial and nuclear plants) have been dynamically analyzed and designed through the mathematical implementation of either elastic or simple nonlinear models such as elastic–plastic, bilinear, modified Clough, Q-hysteresis, Takeda and slip models, [1]. However, many structural systems indicate considerable inelastic behavior with unfavorable hysteretic characteristics such as strength degradation, stiffness degradation, and pinching phenomena when subjected to cyclic excitations. Therefore, the aforementioned simple models are not adequate for structural designers to understand the true inelastic behavior and energy dissipation capability of engineering structures.

Developing an appropriate nonlinear hysteretic model which is able to acceptably portray the highly inelastic response of structural members due to random cyclic excitations would result in better insight into the energy absorbability of various earthquake-resistant systems. The suchlike model could also introduce new concepts to revise the design codes that have been mostly compiled based on circumscribed experimental tests on specific structural configurations and excitation properties. However, this kind of hysteretic model should involve remarkably more complicated mathematical equations. Moreover, it will be a crucial task to incorporate them into the dynamic analysis of structures.

* Corresponding author.
E-mail address: pooya.sareh@liverpool.ac.uk (P. Sareh).

https://doi.org/10.1016/j.dajour.2022.100147
Received 24 September 2022; Received in revised form 27 November 2022; Accepted 30 November 2022
Available online 5 December 2022

Nomenclature

Sym.	Property
k	Initial stiffness
α	Ratio of final tangent stiffness to the initial stiffness
k_f	Final tangent stiffness
u	Relative displacement
z	Hysteretic displacement
β, γ, and n	Unknown basic shape-controlling parameters
ν	Strength degrading functions
η	Stiffness degrading functions
$h(z)$	Pinching function
ε	Hysteretic dissipated energy
δ_ν	Unknown stiffness degrading parameters
δ_η	Unknown stiffness degrading parameters
t	Time duration of system's response at each time instant
sgn(.)	*Signum* function
q	Pinching level
z_u	Ultimate hysteretic displacement
ζ_1 and ζ_2	Pinching controller functions
ζ_s	Parameters for setting pinching shape, rate, and severity
p	Parameters for setting pinching shape, rate, and severity
ψ	Parameters for setting pinching shape, rate, and severity
δ_ψ	Parameters for setting pinching shape, rate, and severity
λ	Parameters for setting pinching shape, rate, and severity
[M]	Structural mass matrices
[C]	Viscous damping matrices
$\{\ddot{x}\}$	Vectors of stories' acceleration
$\{\dot{x}\}$	Vectors of stories' velocity
$\{F(t)\}$	Vector of external excitations
$\{R(u,z)\}$	Vector of stories' hysteretic restoring forces
u	Inter-story drift
$[\Gamma]$	Restoring forces
$[K_f]$	Final tangent stiffness matrix
$k_{\ f}$	Final stiffness for the jth story
$\alpha_j k_{\ j}$	Final tangent stiffness matrix
$\left\{\overline{F(t)}\right\}$	Pseudo-loading vector
$[\Pi]$	Constant diagonal matrix
$\{Z\}$	Vector of stories' hysteretic variables
z_j	Stories' hysteretic variables
Δt	Time-step
$\{x\}_{i+1}^P$	Displacement preliminary solution
$\{\dot{x}\}_{i+1}^P$	Velocity preliminary solution
$\{Z\}_i$	Initial hysteretic variables' values
t_i	Previous time-step
$\dot{u}_j^P$	Preliminary relative velocities of stories
$\{Z\}_{i+1}^P$	Final vector of hysteretic variables' values
$\{S\}_{i+1}$	Final state of the system
$\{Z\}_{i+1}$	Final vector of hysteretic variables' values
E	Acceptable low tolerances
F_k	Resultant force acting on the kth CP
N_{cp}	Number of CPs
fitbest	Best fitness of all the CPs
fitworst	Worst fitness of all the CPs
$fit(I)$	Fitness of agent I
r_{Ik}	Separation distance
X_I	Positions of the I-th cps
X_k	Positions of the kth cps
ε_p	Small positive number
p_{Ik}	Probability of moving
k_a	Acceleration coefficient
k_v	Velocity coefficient
$iter$	Actual iteration number
$iter_{max}$	Maximum number of iterations
k_1	Internal acceleration coefficient
k_2	Internal velocity coefficient
BF_{min}	Minimum fitness values
BF_{max}	Maximum fitness values
$\hat{R}$	Predicted restoring force time-history
R	Experimentally obtained restoring force time-history
X	Vector of BWBN model parameters
σ_f^2	Variance of the experimental restoring force time-history
N_e	Number of used data in the optimization process
N_E	Number of captured experimental data
$X_{\min}$	Lower bound of the model's parameters
$X_{\max}$	Upper bound of the model's parameters

Abbreviations

Abr.	Definition
BWBN	Bouc–Wen–Baber–Noori
CSS	Charged System Search
F-CSS	Fuzzy Adaptive Charged System Search
MCSS	Magnetic CSS
IHA	Iterative Hysteretic Analysis
SDOF	single-degree-of-freedom
YSPD	yielding shear panel devices
CPs	Charged Particles
CP	Charged Particle
CM	Charged Memory
BF	Best Fitness
UBF	Unchanged Best Fitness
FL	Fuzzy Logic
NBF	Normalized Best Fitness
NUBF	Normalized Unchanged Best Fitness

The main contribution of this research work is the development of a procedure to achieve precise simulated hysteresis models required for accurate nonlinear structural analyses. In this paper, the parameter identification of the Bouc–Wen–Baber–Noori (BWBN) constitutive model [1–10] is concerned that involves degrading and pinching characteristics experimentally observed in the nonlinear cyclic behavior of structural members. Furthermore, it is capable of predicting the hysteretic behavior of nonlinear systems resulting from arbitrary external excitations. Some experimental results from previous studies are utilized for comparative purposes while a nonlinear dynamic

analysis process is also provided. The hysteretic behavior of two simply supported steel shear walls under cyclic loading conditions [11] is experimentally investigated as a representative of lateral-resistant structural components (e.g. concrete shear walls, steel braces, and connections). To this end, the Fuzzy Adaptive Charged System Search (F-CSS) [12,13] is developed based on the standard Charged System Search (CSS) [14] optimization algorithm. In this algorithm, a parameter-tuning process based on fuzzy logic is proposed to achieve better performance while using the standard CSS algorithm. To achieve this aim, four linguistic variables are defined which configure a fuzzy system for parameter identification in the standard CSS algorithm. The F-CSS algorithm is applied to an optimization problem in which the parameter identification of the BWBN constitutive model is concerned.

In recent years, a wide range of nature- and physics-inspired metaheuristic algorithms [15–27] have been proposed for dealing with different mechanical and structural design problems [28–41]. More specifically, a variety of methods have been proposed by researchers to improve the searching capabilities of standard metaheuristic algorithms [42–63]. The majority of existing improved versions of the CSS algorithm have been shown to be efficient and robust in solving highly nonlinear system identification problems [12,64]. In this study, a two-degree-of-freedom shear wall building example is solved using the results of the proposed F-CSS method, and a discussion of the results is presented. These results are also compared to the results of the standard CSS [14] and the Magnetic CSS (MCSS) [65,66] algorithms.

This paper is organized into two major parts including "system identification of hysteretic structural models" (Section 2 to 5) and "development of optimization process for hysteretic simulation" (Sections 6 and 7). Section 2 presents a complete description of the BWBN constitutive model. The problem under examination and related experimental findings are described in Section 3. An innovative hysteretic time-history analysis process called Iterative Hysteretic Analysis (IHA) is proposed and presented in Section 4 for the nonlinear analysis of multi-degree-of-freedom (MDOF) structural systems. The statement of the optimization problem and the obtained numerical results are presented in Sections 5 and 6, respectively. Finally, concluding remarks and suggestions for future research are presented in Section 7.

2. Description of the BWBN model

Bouc [67] suggested a versatile and smooth hysteresis model for an inelastic single-degree-of-freedom (SDOF) system subjected to forced vibration, and subsequently Wen [68] generalized Bouc's hysteretic constitutive law and developed an approximate solution procedure for random vibrations. Following that, the Bouc–Wen model has been widely used as a mathematical description of physical systems with hysteresis and nonlinear behavior, especially for problems in civil and mechanical engineering. In this model, the nonlinear restoring force is related to the system's deformation through a first-order nonlinear differential equation, which has a set of unknown shape parameters. Baber and Wen [69] extended the Bouc–Wen model to consider degradations in the strength and stiffness of structural systems by introducing new unknown degrading parameters in terms of the dissipated hysteretic energy. Baber and Noori [70] expanded this version of the pinching phenomenon by incorporating a pinching function into the preceding model which is also a function of dissipated hysteretic energy and possesses further unknown parameters. Foliente [2,3] developed a more efficient pinching function based on the experimental observations of structural elements' hysteretic behavior and provided a modified BWBN model, which is utilized in the present study.

Although the exact physical meanings of all parameters in the so-called Bouc–Wen models are not thoroughly specified so far, each parameter has been introduced through a distinct interpretation and plays a specific role in forming the characteristics of the hysteretic behavior observed in experiments. A detailed discussion on this topic could be found in [2]. By determining and substituting the optimal values of unknown parameters, the response of various Bouc–Wen models could convincingly match the experimentally observed behavior of many hysteretic structural components. The standard Bouc–Wen model has been used to recreate the non-pinching and non-degrading hysteretic behavior of steel beams [71,72], base isolators [73], magneto-rheological damper [74,75], mild steel dampers [76], and cracked piles [77]. Furthermore, the BWBN model has been employed to simulate the degrading and pinching hysteresis of wood joints [3], reinforced concrete elements, timber shear walls, wooden T-connections, and yielding shear panel devices (YSPD) [10]. Moreover, the BWBN model has effectively been integrated into a stochastic ground motion model for predicting the stochastic response of high nonlinear structures under seismic excitations using the probability density evolution method. A comprehensive survey on the applications of the Bouc–Wen models in modeling the hysteretic behavior of mechanical systems can be found in Ref. [78].

The total hysteretic, pinching, and degrading nonlinear restoring force described by the BWBN model comprises a purely linear and a hysteretic term and is calculated as follows

$$R(u,z) = \alpha k u + (1-\alpha) k z \tag{1}$$

where k is initial stiffness, α is the ratio of final tangent stiffness (k_f) to initial stiffness [2], u is relative displacement, and z is hysteretic displacement. By eliminating the one-degree redundancy existing in the Bouc–Wen model using a freezing technique described in [5], z can be expressed as follows

$$\dot{z} = h(z)\left\{\frac{\dot{u} - \nu\left(\beta|\dot{u}||z|^{n-1}z + \gamma\dot{u}|z|^{n}\right)}{\eta}\right\} \tag{2}$$

where β, γ, and n are the unknown basic shape-controlling parameters of the Bouc–Wen model, ν and η denote the strength and stiffness degrading functions, respectively, and $h(z)$ is the pinching function. The degrading and pinching functions are dependent on the severity and duration of the response; therefore, they are defined as the functions of hysteretic dissipated energy ε. Based on empirical observations, the degrading functions are assumed to be linear functions of the dissipated energy as follows

$$\nu(\varepsilon) = 1 + \delta_\nu \varepsilon \tag{3}$$

$$\eta(\varepsilon) = 1 + \delta_\eta \varepsilon \tag{4}$$

where δ_ν and δ_η are unknown strength and stiffness degrading parameters in which the hysteretic dissipated energy, ε, is specified as

$$\varepsilon(t) = \int_0^t z\dot{u}dt \tag{5}$$

where t denotes the time duration of the system's response at each time instant.

The pinching function is also derived from experimental observations about the hysteretic behavior of structural systems and is defined by the following equation [2,3]

$$h(z) = 1 - \zeta_1 e^{-\left[z\,\mathrm{sgn}(\dot{u}) - q z_u\right]^2/\zeta_2^2} \tag{6}$$

where sgn(.) is the *signum* function, and unknown parameter q sets the pinching level as a fraction of ultimate hysteretic displacement, z_u, which is calculated from the following equation

$$z_u = \left(\frac{1}{\upsilon(\beta+\gamma)}\right)^{\frac{1}{n}} \tag{7}$$

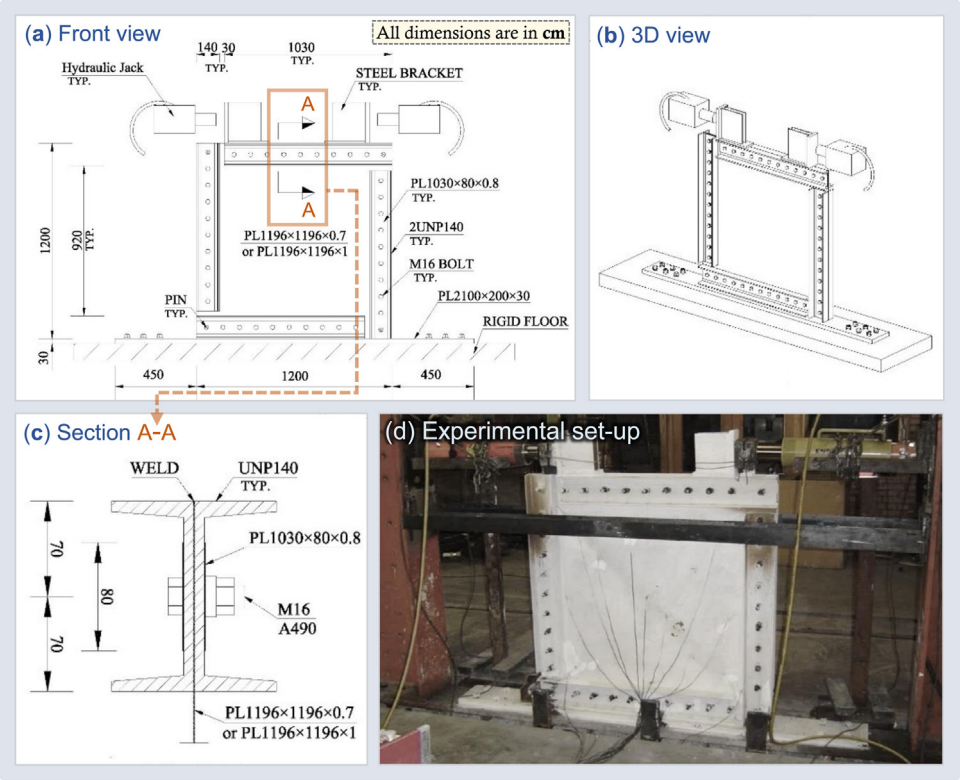

Fig. 1. (**a** to **c**) Technical drawings of the specimens. (**d**) Experimental test set-up [11].

and ζ_1 and ζ_2 are pinching controller functions which are formulated as follows

$$\zeta_1(\varepsilon) = \zeta_s\left[1 - e^{(-p\varepsilon)}\right] \tag{8}$$

$$\zeta_2(\varepsilon) = \left(\psi + \delta_\psi \varepsilon\right)\left(\lambda + \zeta_1\right) \tag{9}$$

In the abovementioned equations, five unknown parameters ζ_s, p, ψ, δ_ψ and λ set pinching shape, rate, and severity. The BWBN model encompasses all the significant features observed in the experimentally observed hysteretic behavior of structural elements including the strength degradation, stiffness degradation, and pinching of the successive hysteresis loops [2,3,7].

By adjusting the twelve unspecified parameters of the BWBN model, i.e. α, β, γ, n, δ_ν, δ_η, q, ζ_s, p, ψ, δ_ψ, and λ, it is possible to reproduce the experimental response of structural hysteretic components to any random excitations. It is important to mention that this process should be gone through by solving an optimization problem with the objective of fitting the model's response to the experimentally obtained data.

3. Description of experimental findings

Herein, the experimental observations about two simply-supported steel shear walls are taken into consideration as representatives of lateral-resistant structural systems. The objective is to identify the optimal parameters set of the BWBN model for these walls by solving an optimization problem. The resulting model is then capable of predicting the hysteretic response of these steel shear walls under any external excitation and is valid for being actively utilized in the accurate nonlinear analysis of the corresponding MDOF system.

3.1. Test set-up

Two simply-supported steel shear walls with shear panels thickness of 0.7 mm (Specimen A) and 1 mm (Specimen B) were examined under cyclic loadings [11]. As illustrated in Fig. 1a–c, the internal plate dimensions of the specimens are 920 mm × 920 mm. The boundary members are 2UNP140 strengthened by two 1030 mm × 80 mm × 8 mm plates on both sides of their webs and pin joints are used at beam-to-column connections. Steel panels were fixed on the boundary members by frictional A490 bolts and the corner bolts were left unfastened to ensure proper hinge performance. Specimens were fixed on a rigid floor using a 2100 mm × 200 mm × 30 mm plate welded by two lines of 8-mm fillet welding. Moreover, two welded steel brackets were included on the top of the story beam at each side and connected to hydraulic jacks for the application of lateral cyclic loads.

Fig. 1d indicates a specimen under test conditions including the connection details of hydraulic jacks to the steel brackets for the application of lateral cyclic loads. It also depicts the out-of-plane bracings of the boundary elements which prevent the top boundary member's buckling to simulate the floor rigid diaphragm performance. The mechanical characteristics of the 0.7-mm and 1-mm steel panels used in Specimens A and B were obtained through standard tensile tests as follows [11]:

$$\text{Specimen A}: \begin{cases} F_y = 266\ \text{MPa} \\ F_u = 330\ \text{MPa} \\ E = 200\ \text{GPa} \\ \mu = 0.3 \end{cases} \quad \text{and} \quad \text{Specimen B}: \begin{cases} F_y = 228\ \text{MPa} \\ F_u = 370\ \text{Mpa} \\ E = 200\ \text{GPa} \\ \mu = 0.3 \end{cases}$$

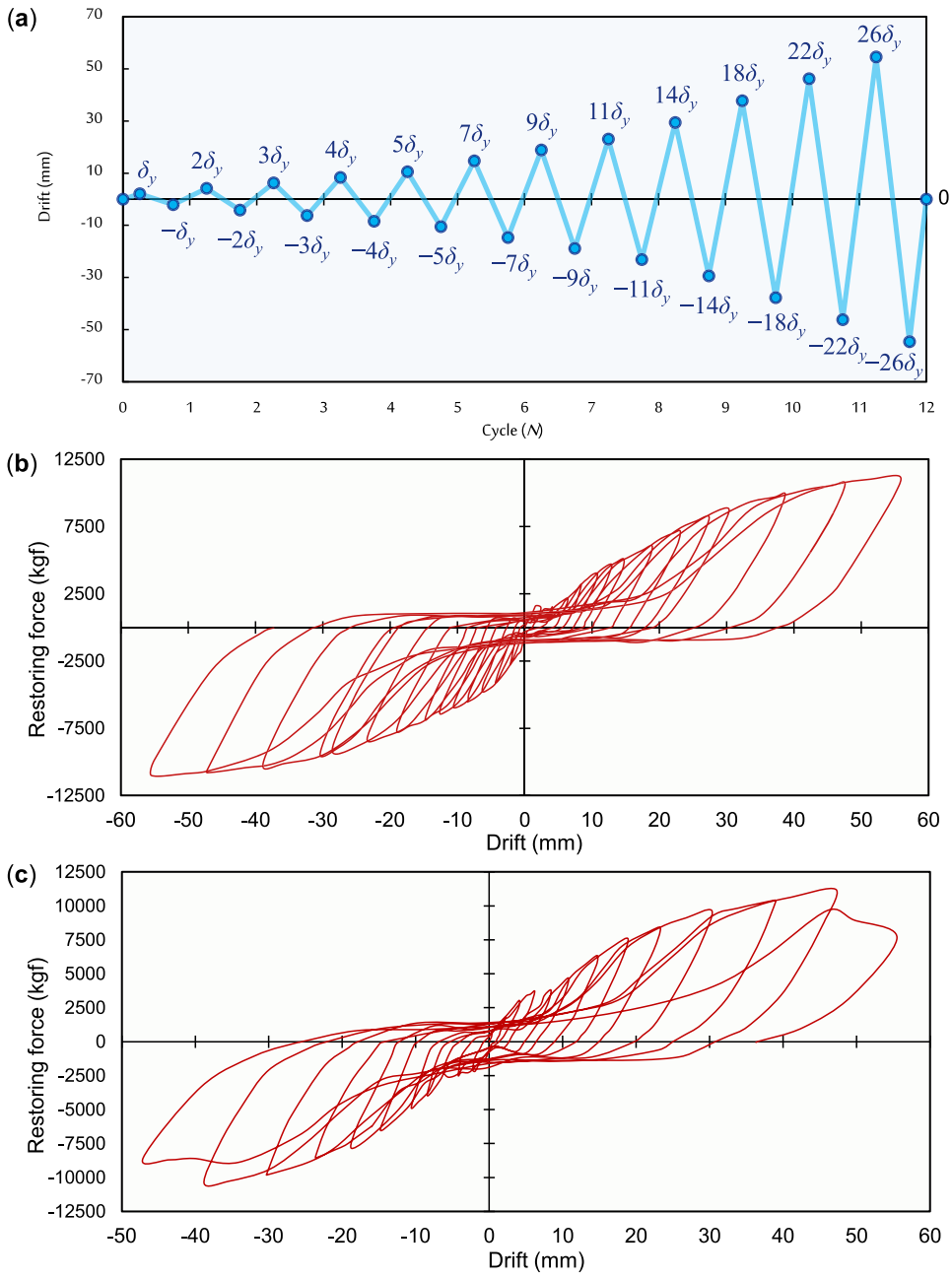

Fig. 2. (**a**) Target drift pattern for the experiments.(**b**) Experimental hysteresis loops for Specimen A.(**c**) Experimental hysteresis loops for Specimen B. *Source:* (adapted from [11]).

where F_y and F_u represent yielding and ultimate strengths, respectively, and E and μ denote modulus of elasticity and Poisson's ratio, respectively.

3.2. Experimental data

The steel brackets were arranged to be repeatedly loaded, unloaded, and negatively loaded by opposite hydraulic jacks to inversely reach multipliers of the theoretically calculated yielding displacement of the specimens (δ_y = 2.1 mm) as the predefined target drifts according to the pattern illustrated in Fig. 2a until failure takes place. Since the variations of the captured restoring forces would be slight for further nonlinear cycles, the target drift increment was progressively increased after $5\delta_y$ to significantly reduce the test time costs.

The achieved drift-force hysteresis loops for Specimens A and B are presented in Fig. 2b and c, respectively. It is observed that the steel shear walls show an extremely high nonlinear behavior as the yielding point is not recognizable; also, stiffness and strength degradations do not appear in their hysteretic behavior, and the hysteresis loops are pinched at approximately the mid-drift of each loading–unloading cycle.

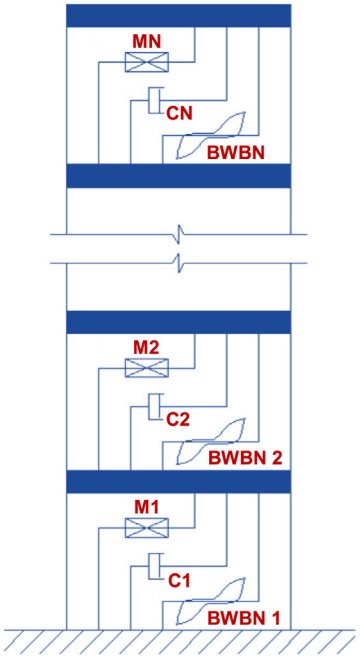

Fig. 3. Schematic representation of the N-DOF nonlinear hysteretic shear building.

4. Nonlinear structural analysis

A complex optimization process, in general, requires a large number of function evaluations, and connecting this process with non-linear analysis software such as OpenSees introduces significant additional computational cost and complexity to the numerical investigation. To deal with such a challenge, here we propose a structural analysis process called *Iterative Hysteresis Analysis* (*IHA*), the details of which are described in this section.

It is important to note that the identification of structural response to arbitrary dynamic loadings, such as cyclic and earthquake-type loadings, can lead to several advantages; examples include the recognition of energy-dissipating mechanisms, fatigue, and the failure modes of structural systems subjected to dynamic loadings where the verified hysteretic models are available and the hysteretic behavior of various structural systems are known [3]. Herein, a simple nonlinear analysis method based on the hysteretic behavior of the structural lateral-resisting components described by the BWBN constitutive law is introduced for the nonlinear hysteretic time-history analysis of MDOF structural systems. Through the utilization of the BWBN model for the description of the lateral resistant element's restoring force, and using D'Alembert's principle, the equation of motion for an N-degree-of-freedom nonlinear shear building, as depicted in Fig. 3, can be given as

$$[M]_{N\times N}\{\ddot{x}\}_{N\times 1}+[C]_{N\times N}\{\dot{x}\}_{N\times 1}+[\Gamma]_{N\times N}\{R(u,z)\}_{N\times 1}=\{F(t)\}_{N\times 1} \tag{10}$$

where $[M]$, $[C]$, $\{\ddot{x}\}$, and $\{\dot{x}\}$ denote structural mass, viscous damping matrices, and the vectors of stories' acceleration and velocity in relation to the ground, respectively; $\{F(t)\}$ is the vector of external excitations affecting building stories; $\{R(u,z)\}$ is the vector of stories' hysteretic restoring forces calculated by Eq. (1) for each story (it should be noticed that u signifies the inter-story drift calculated for each story as $u_j = x_{j+1} - x_j$); and, matrix $[\Gamma]$ determines the restoring forces that affect each story the elements of which are defined as

$$\begin{cases}\Gamma(j,j)=1 \quad \text{for} \quad j=1\sim N\\ \Gamma(w,w+1)=-1 \quad \text{for} \quad w=1\sim(N-1)\end{cases} \tag{11}$$

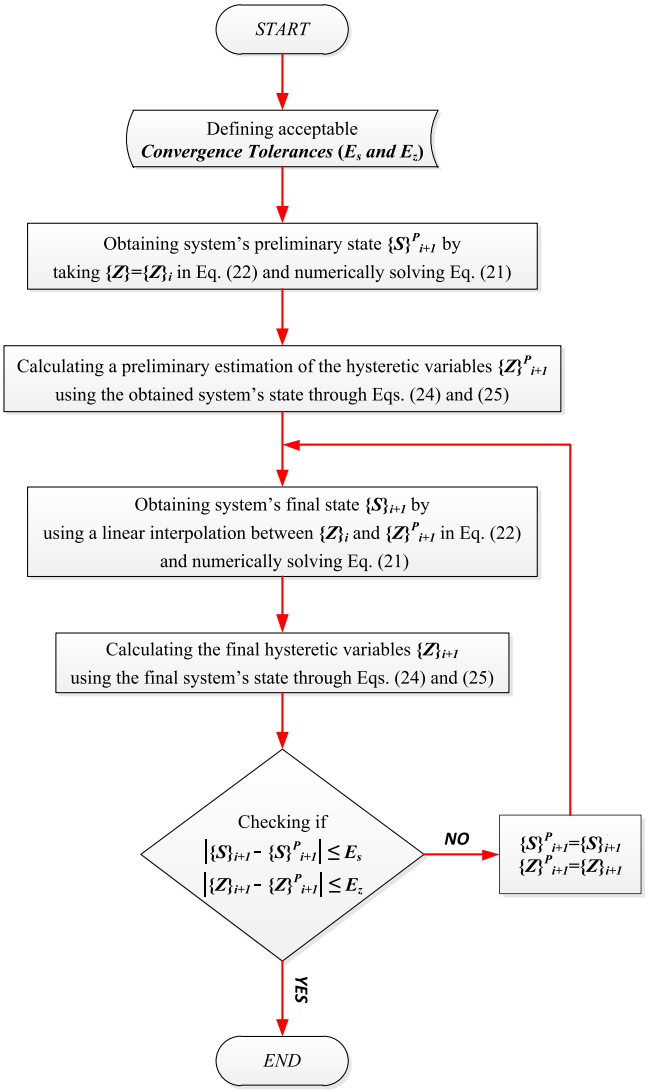

Fig. 4. Flowchart of the nonlinear structural analysis process.

Recalling the BWBN model's equations, the equation of motion of the system (Eq. (10)) can be simplified and rearranged as

$$[M]_{N\times N}\{\ddot{x}\}_{N\times 1}+[C]_{N\times N}\{\dot{x}\}_{N\times 1}+[K_f]_{N\times N}\{x\}_{N\times 1}=\left\{\overline{F(t)}\right\}_{N\times 1} \tag{12}$$

where $[K_f]$ is the final tangent stiffness matrix. Note that the final stiffness for the jth story k_f should be calculated as $\alpha_j k_j$, and the final tangent stiffness matrix is arranged similarly to the standard linear stiffness matrix. Furthermore, $\left\{\overline{F(t)}\right\}$ is the pseudo-loading vector formulated as

$$\left\{\overline{F(t)}\right\}_{N\times 1}=\{F(t)\}_{N\times 1}-[\Gamma]_{N\times N}[\Pi]_{N\times N}\{Z\}_{N\times 1} \tag{13}$$

where $[\Pi]$ is a constant diagonal matrix that is formed as follows

$$\Pi(j,j)=(1-\alpha_j)k_j \quad \text{for} \quad j=1\sim N \tag{14}$$

and $\{Z\}$ is the vector of stories' hysteretic variables z_j which are calculated for each story by the following BWBN constitutive law

$$\dot{z}_j=h_j(z_j)\left\{\frac{\dot{u}_j-\nu_j\left(\beta_j|\dot{u}_j||z_j|^{n_j-1}z_j+\gamma_j\dot{u}_j|z_j|^{n_j}\right)}{\eta_j}\right\}, \quad j=1\sim N \tag{15}$$

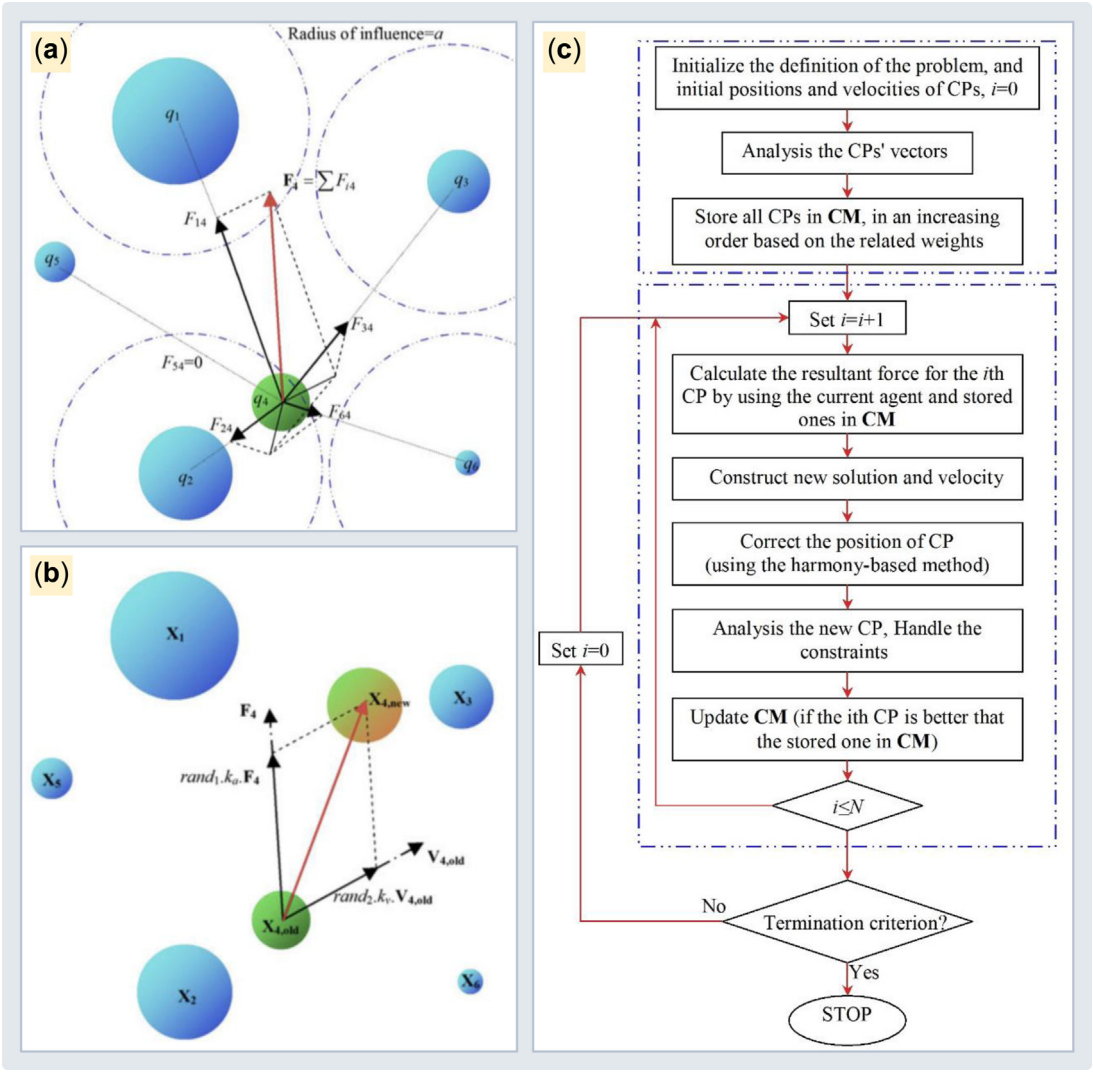

Fig. 5. (**a**) Determination of the resultant electrical force acting on a CP [14]. (**b**) Schematic representation of a CP moving to a new position [14]. (**c**) Flowchart of CSS.

which is governed by the following set of equations in which damping is calculated

$$\begin{cases} v_j(\varepsilon) = 1 + \delta_{vj}\varepsilon_j, \\ \eta_j(\varepsilon) = 1 + \delta_{\eta j}\varepsilon_j, \\ h_j(z_j) = 1 - \zeta_{1j} e^{-\left[z_j \operatorname{sgn}(\dot{u}_j) - q_j z_{uj}\right]^2 / \zeta_{2j}^2}, \\ \varepsilon_j(t) = \int_0^t z_j \dot{u}_j dt, \\ \dot{u}_j = \dot{x}_{j+1} - \dot{x}_j, \\ z_{uj} = \left(\dfrac{1}{v_j \left(\beta_j + \gamma_j\right)} \right)^{\frac{1}{nj}}, \\ \zeta_{1j}(\varepsilon_j) = \zeta_{sj}\left[1 - e^{-p_j \varepsilon_j}\right], \\ \zeta_{2j}(\varepsilon_j) = \left(\psi_j + \delta_{\psi j}\varepsilon_j\right)\left(\lambda_j + \zeta_{1j}\right). \end{cases} \quad , \quad j = 1 \sim N \tag{16}$$

Herein, the following programming stages are undertaken to calculate the system's time-history response by computing a numerical solution for Eq. (12) at each short time step ($\Delta t = t_i + 1 - t_i$) in which the external excitation can be simplified and expressed as a linear relation.

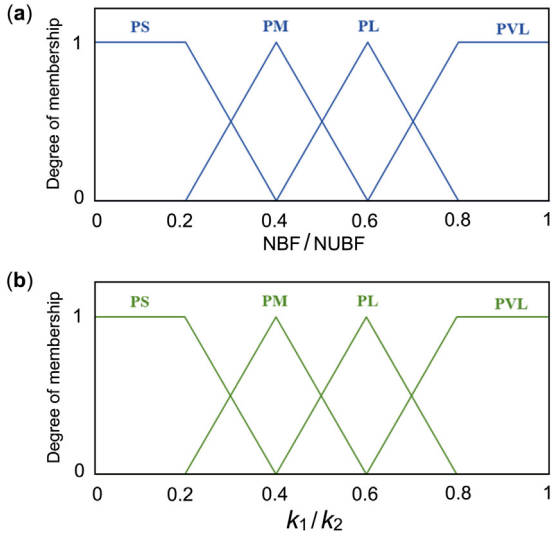

Fig. 6. (**a**) Fuzzy input membership functions. (**b**) Fuzzy output membership functions.

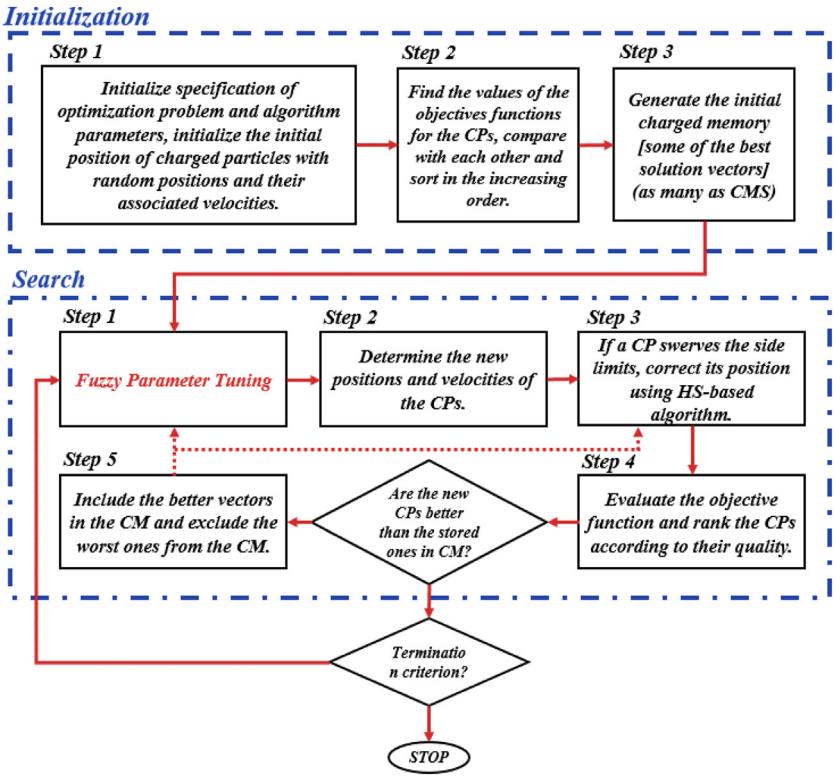

Fig. 7. Flowchart of F-CSS.

Step 1: A preliminary solution, i.e. $\{x\}_{i+1}^{P}$ and $\{\dot{x}\}_{i+1}^{P}$, of Eq. (12) is numerically calculated by assuming a linear interpolation function for the external excitation as [79]

$$\{F(t)\} = \frac{\{F(t_{i+1})\} - \{F(t_i)\}}{\Delta t} t + \{F(t_i)\} \tag{17}$$

and by substituting the constant vector of initial hysteretic variables' values $\{Z\}_i$ obtained at the end of the previous time step t_i for $\{Z\}$ in Eq. (13). In fact, it is assumed that the applied load is gradually applied by very small time increments of Δt, during which, the external force can be assumed to change linearly. At this stage, a preliminary state of the system is achieved as follows

$$\{S\}_{i+1}^{P} = \begin{Bmatrix} \{x\}_{i+1}^{P} \\ \{\dot{x}\}_{i+1}^{P} \end{Bmatrix} \tag{18}$$

Step 2: The preliminary relative velocities of stories ($\dot{u}_j^P$) are specified by means of the preliminary solution obtained in the previous stage and employed by Eqs. (24) and (25) to find a preliminary estimation of the final vector of hysteretic variables' values $\{Z\}_{i+1}^{P}$ at t_{i+1}.

Step 3: At this time, the solution of Eq. (21) is numerically calculated by taking a linear interpolation function of hysteretic variables over the time step in Eq. (22) as $\{Z\} = \frac{\{Z\}_{i+1}^{P} - \{Z\}_i}{\Delta t} t + \{Z\}_i$ to account for the dependency of hysteretic variables on time [80]. Thus, the final state of the system, $\{S\}_{i+1} = \begin{Bmatrix} \{x\}_{i+1} \\ \{\dot{x}\}_{i+1} \end{Bmatrix}$, is obtained.

Step 4: The obtained final state of the system is directly used to calculate the final vector of hysteretic variables' values $\{Z\}_{i+1}$ using Eq. (16).

Step 5: Acceptable low tolerances (E) are defined for discrepancies between preliminary and final solutions as stopping criteria, and the analysis is continued by the following conditional laws until the stopping criteria are met and the convergence is achieved

$$\begin{cases} \text{if} \begin{cases} \left|\{S\}_{i+1} - \{S\}_{i+1}^{P}\right| \le E_s \\ \& \\ \left|\{Z\}_{i+1} - \{Z\}_{i+1}^{P}\right| \le E_z \end{cases} \Rightarrow \text{the final solutions are accepted,} \\ \text{else} \Rightarrow \text{take} \begin{cases} \{S\}_{i+1}^{P} = \{S\}_{i+1} \\ \& \\ \{Z\}_{i+1}^{P} = \{Z\}_{i+1} \end{cases} \text{and iteratively go to } \textbf{Step3}. \end{cases} \tag{19}$$

Fig. 4 demonstrates the programming flowchart of the nonlinear structural analysis. In this process, the structural equation of motion and the nonlinear differential equation of the BWBN model are solved separately and integrated subsequently until convergence is achieved. As such, a computer program that solves the BWBN differential equations can be written and linked to the commercial finite element software, e.g. Abaqus and SAP2000, to easily incorporate the discussed method. As it can be found from Eq. (12), in this process, hysteretic variables Z_j are assumed to act on the system in the opposite direction which has been already used for a number of structural systems employing the Bouc–Wen hysteretic model [80,81]. In another word, the hysteretic variables are initially assumed to be loaded on the system and then will be repeatedly corrected based on the obtained system's state (feedback response), leading to obtaining their true values. Note that, the mentioned analysis approach can also be easily adapted to any other hysteretic models in which the hysteretic variables are calculated from different equations of the BWBN model (Eqs. (15) and (16)).

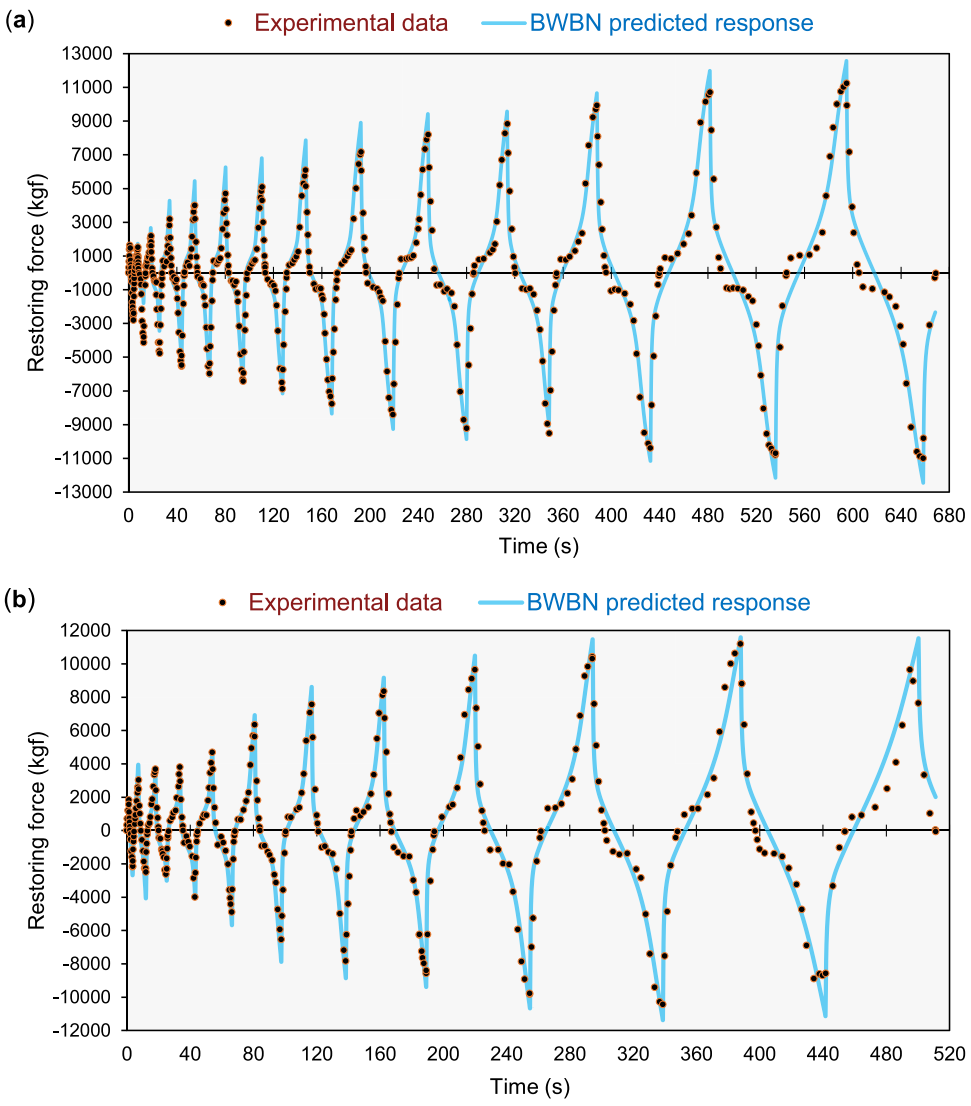

Fig. 8. Comparison between the experimental restoring force and the BWBN model's predicted force for (**a**) Specimen A, and (**b**) Specimen B.

5. Statement of the optimization procedure

5.1. Standard CSS

As mentioned before, some principles of physics and mechanics are utilized in the formulation of the CSS algorithm. The pseudo-code for the CSS algorithm can be summarized as follows.

Step 1: ***Initialization***. The initial positions of *Charged Particles* (*CPs*) are determined randomly in the search space, whereas their initial velocities are assumed to be zero. A number of the best CPs and their related values of the fitness function are saved in a memory called *Charged Memory* (*CM*).

Step 2: ***Forces determination***. The value of the resultant electrical force acting on a Charged Particle (CP) is specified as follows where the resultant force acting on the jth CP is illustrated in Fig. 5a.

$$\mathbf{F}_k = q_k \sum_{I,\, I\neq k} \left(\frac{q_I}{a^3} r_{Ik} \cdot i_1 + \frac{q_I}{r_{Ik}^2} \cdot i_2 \right) \times a r_{Ik} p_{Ik} (\mathbf{X}_I - \mathbf{X}_k) \qquad \begin{cases} k = 1, 2, \ldots, N_{cp} \\ i_1 = 1, i_2 = 0 \Leftrightarrow r_{Ik} < a \\ i_1 = 0, i_2 = 1 \Leftrightarrow r_{Ik} \geq a \end{cases} \tag{20}$$

where F_k is the resultant force acting on the kth CP and N_{cp} is the number of CPs.

The magnitude of charge, q_I, for each CP, considering the quality of its solution, is defined as

$$q_I = \frac{fit(I) - fitworst}{fitbest - fitworst}, \quad I = 1, 2, \ldots, N_{cp} \tag{21}$$

where *fitbest* and *fitworst* are the best and the worst fitness of all CPs, respectively; $fit(I)$ represents the fitness of agent I; and N_{cp} is the total number of CPs. The separation distance r_{Ik} between two charged particles is defined as follows

$$r_{Ik} = \frac{\|\mathbf{X}_I - \mathbf{X}_k\|}{\|(\mathbf{X}_I + \mathbf{X}_k)/2 - \mathbf{X}_{best}\| + \varepsilon p} \tag{22}$$

where X_I and X_k are the positions of the Ith and kth CPs, respectively, X_{best} is the position of the best current CP, and ε_p is a small positive number to avoid singularities. Here, p_{Ik} is the probability of moving each CP towards the others as described in [14].

Step 3: ***Solution construction.*** Each CP moves to the new position using the resultant force and velocity vector as shown in Fig. 5b, calculated as

$$\mathbf{X}_{k,new} = rand_{k1} \cdot k_a \cdot \mathbf{F}_k + rand_{k2} \cdot k_v \cdot \mathbf{V}_{k,old} + \mathbf{X}_{k,old} \tag{23}$$

$$\mathbf{V}_{k,new} = \mathbf{X}_{k,new} - \mathbf{X}_{k,old} \tag{24}$$

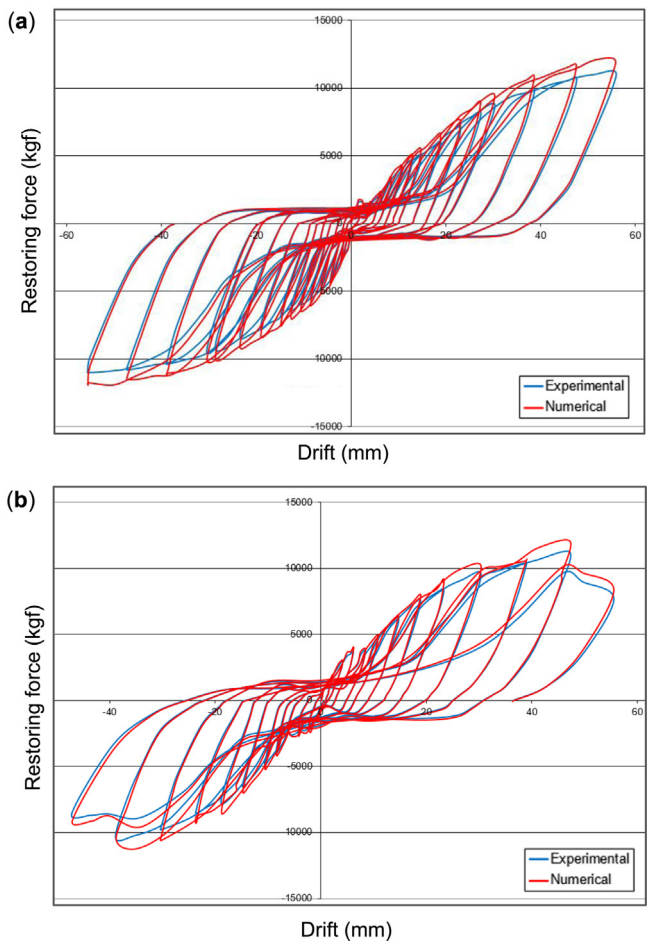

Fig. 9. Force–displacement curves of the experimental and numerical investigations for (**a**) Specimen A, and (**b**) Specimen B.

where k_a is the acceleration coefficient; k_v is the velocity coefficient to control the influence of the previous velocity; and $rand_{k1}$ and $rand_{k2}$ are two random numbers uniformly distributed in the range of (0,1).

Step 4: ***Updating process***. If a new CP exits from the allowable search space, a harmony search-based handling approach is used to correct its position [14]. In addition, if some new CP vectors are better than the worst ones in the CM, they will replace the worst ones in the CM.

Step 5: ***Terminating criterion control***. Steps 2–4 are repeated until a terminating criterion is satisfied. The terminating criterion is one of the following conditions (the one that occurs earlier):

(1) *Maximum distance of CPs*: the maximum distance between CPs is less than a pre-determined value (3×a in this paper); or

(2) *The maximum number of iterations*: the optimization process is terminated after a fixed number of iterations. Fig. 5c shows the flowchart of the CSS algorithm.

5.2. Fuzzy adaptive CSS (F-CSS)

Two important parameters have considerable importance in the exploration and exploitation tuning of the standard CSS algorithm. As mentioned in Eq. (23), k_v and k_a are utilized to consider and tune the effects of the previous velocity of each CP and the resultant force acting on that CP. The exploration capability of the algorithm is improved based on the excessive search in the initial iterations while it should be decreased due to the exploitation requirements of the algorithm. Given that k_a is a parameter related to the attracting forces on CPs, considering a larger value for this parameter may result in a fast convergence rate, whereas a smaller value can increase the computational complexity and time of the algorithm. It should be noted that k_a controls the exploitation phase of the algorithm which requires is of great importance; hence, determining an incremental function can enhance the overall performance of the algorithm in this phase. In addition, the direction of the previous velocity of a CP is not generally the same as the resultant force; therefore, considering a decreasing function for the determination of k_v which controls the exploration phase of the algorithm is required.

Table 1
Fuzzy linguistic variables.

Fuzzy variable	Variable description
PS	Positive & Small
PM	Positive & Medium
PL	Positive & Large
PVL	Positive & Very Large

Based on previous studies utilizing CSS as the optimization algorithm, the following equations are used for k_v and k_a, while k_1 and k_2 are assumed to be 0.5

$$k_a = k_1\left(1 - \frac{iter}{iter_{\max}}\right), \tag{25}$$

$$k_v = k_2\left(1 + \frac{iter}{iter_{\max}}\right), \tag{26}$$

where $iter$ is the actual iteration number and $iter_{max}$ is the maximum number of iterations. Considering these equations, k_v decreases linearly to zero whereas k_a increases to one when the number of iterations rises.

Since there is no systematic approach to identifying k_1 and k_2 during the optimization process, there should be an appropriate parameter-tuning process to achieve acceptable levels of performance in dealing with different optimization problems. Due to the lack of knowledge about specific search spaces, designing a mathematical model for the tuning process is generally difficult and time-consuming. Using appropriate linguistic descriptions of the search space leads to a tuning process that can cope with its complexity. Fuzzy Logic (FL) is one of the linguistic-based theories that can contribute to achieving such a goal. In this section, a parameter-tuning process based on FL is proposed to achieve a better performance level for the CSS algorithm. In this regard, four linguistic variables are defined as summarized in Table 1.

The FL tuning process is formulated for k_1 and k_2 independently. This process is conducted based on the Best Fitness (BF) values and the number of Unchanged Best Fitness (UBF) values during each iteration. The FL tuning process is comprised of two input and one output variables. The input variables are chosen as the Normalized Best Fitness (NBF) and Normalized Unchanged Best Fitness (NUBF) values. The fuzzy output variables are chosen as k_1 and k_2. The NBF and NUBF values are calculated as follows

$$NBF = (BF - BF_{\min})/(BF_{\max} - BF_{\min}), \tag{27}$$

$$NUBF = 1 - \left(\frac{iter_{\max} - UBF}{iter_{\max}}\right), \tag{28}$$

where $BF_{\min}$ and $BF_{\max}$ are, respectively, the minimum and maximum fitness values during each iteration.

The fuzzy inputs and output membership functions are represented in Fig. 6a and b, respectively. The fuzzy rule base is also summarized in Table 2. It should be noted that the Mamdani Inference mechanism is utilized for decision making while the centroid method is also chosen for the defuzzification process.

The contribution of the proposed adaptive method proves the fact that the determination of the heuristic parameters is assigned to the

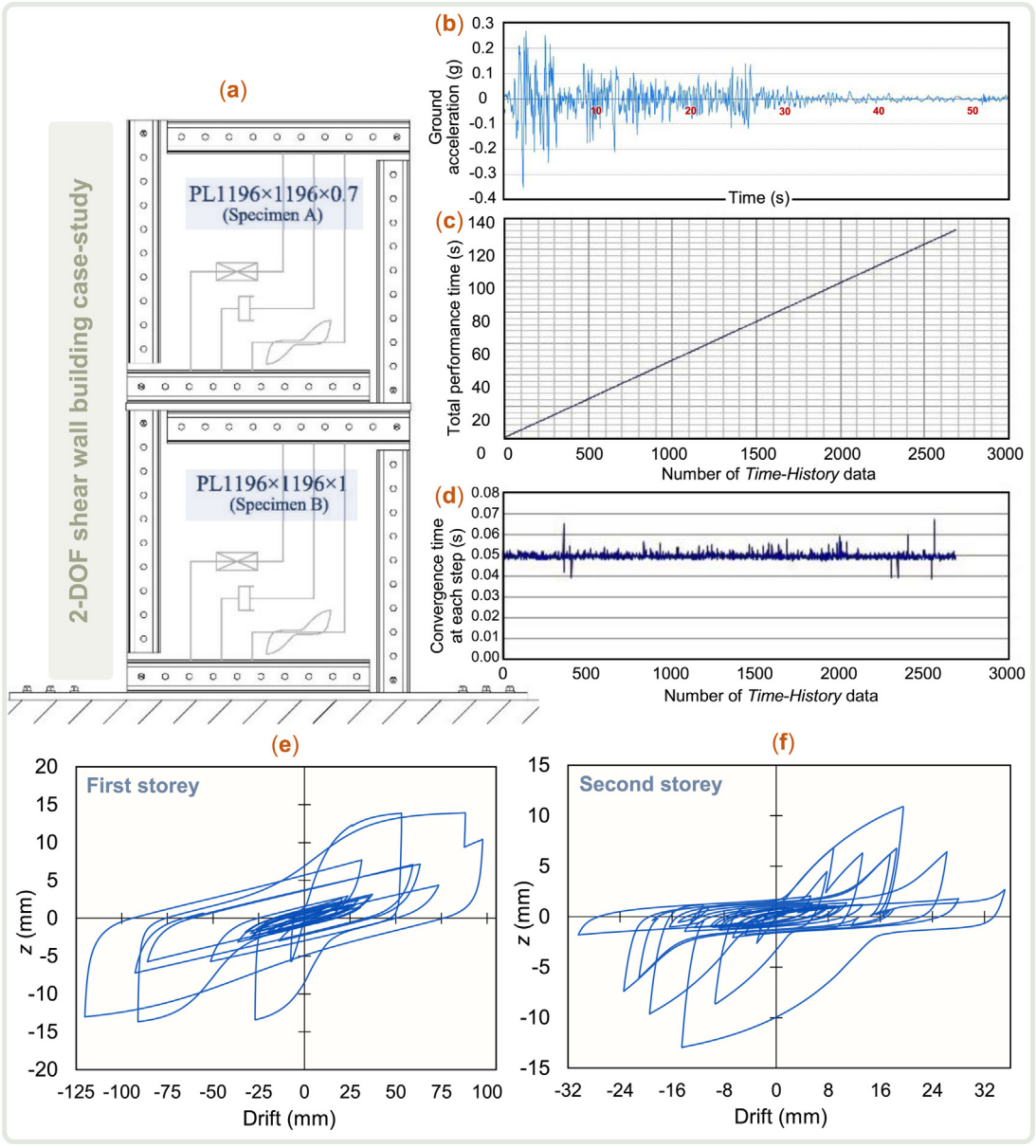

Fig. 10. (**a**) The 2-DOF shear wall building case study. (**b**) The El Centro 1940 earthquake acceleration record. (**c**) The total step convergence time for the hysteretic analysis. (**d**) The maximum step convergence time for the hysteretic analysis. (**e** & **f**) Hysteresis loops of hysteretic displacement versus drift for (**e**) the first, and (**f**) the second stories.

Table 2
Fuzzy rule base.

k_1 / k_2		NUBF			
		PS	PM	PL	PVL
NBF	PS	NVS	NVS	NS	NM
	PM	NVS	NS	NS	NM
	PL	NS	NS	NM	NL
	PVL	NS	NM	NL	NVL

fuzzy system, in contrast to the traditional practice of running numerous experiments. The flowchart of the F-CSS algorithm is presented in Fig. 7.

In the following, the F-CSS identification approach is used to configure the Bouc–Wen–Baber–Noori model's parameters so that the model's responses satisfactorily match the obtained experimental data for steel shear wall subjects. This is achieved by minimizing a suitably defined objective function by solving an optimization problem. It is noteworthy that the F-CSS optimization method is effectively used in the present study to develop an effective tool for solving this high nonlinear parametric identification problem compared to the standard CSS [14]and Magnetic CSS (MCSS) [65] algorithms. Solving this kind of highly nonlinear optimization problem has been always challenging in terms of robustness and converge-ability of the identification method, and F-CSS as a robust and effective algorithm [12–14] can be successfully employed for this purpose.

5.3. Objective function

In order to obtain the optimal values for the parameters of the BWBN model, an appropriate fitness function is needed to be minimized through an optimization procedure. In the present study, the normalized mean square error (NMSE) of the predicted restoring force time-history $\hat{R}$ (for any obtained parameters' vector **X**) in comparison

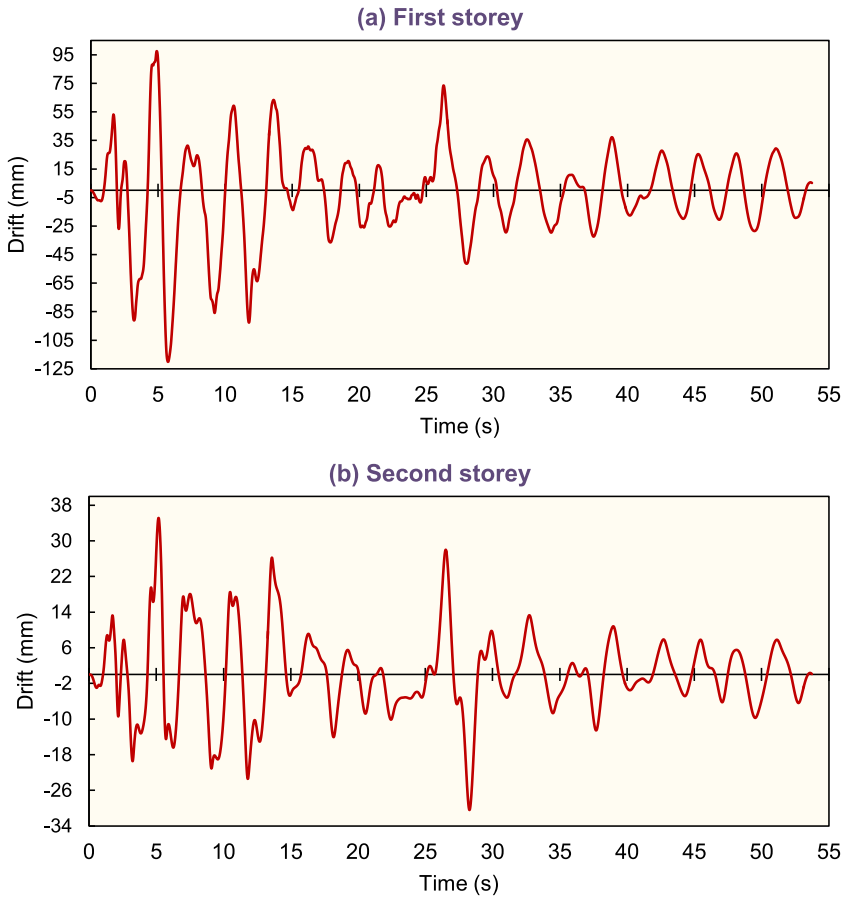

Fig. 11. Drift-time diagrams for the (**a**) first, and (**b**) second stories.

with the experimentally obtained restoring force time-history R at each time instant, is considered as the objective function [74,75]. Thus, the discrete objective function is formulated as

$$NMSE(\mathbf{X}) = \frac{1}{N_e}\sum_{ne=1}^{Ne}\frac{(R-\hat{R})^2}{\sigma_f^2} \tag{29}$$

where $\mathbf{X}$ is the vector of the BWBN model parameters that contains the candidate values of the twelve parameters; σ_f^2 is the variance of the experimental restoring force time-history; and N_e is the number of used data in the optimization process that could be equal to or less than the number of captured experimental data N_E. For optimization operations, in parallel with produced force, the time-history of excitations (i.e., displacement and velocity) is also required to calculate the model's response.

5.4. Bound constraints

In general, the optimization problem involves the minimization of the above objective function when the parameters vector is varied between the following bound constraints (search domain)

$$\mathbf{X}_{\min} \le \mathbf{X} \le \mathbf{X}_{\max} \tag{30}$$

where $\mathbf{X}_{\min}$ and $\mathbf{X}_{\max}$ are vectors containing the lower and upper bounds of the model's parameters, respectively. In [4], a part of the experimental data was used for the system identification of timber structures where it was shown that the model response is robust for the remaining time-history. Moreover, for an MR damper in [74], the obtained parameters due to sinusoidal excitation were successfully exploited for reproducing the damper's response to random excitations. Table 3 presents the search domain of the unknown parameters of the BWBN model implemented for both Specimens A and B which can be estimated through the experimental data analysis described below. It should be noted that the bound limits reported in Table 3 are conservatively widened out and considered to be the same for both specimens.

The parameters are described as follows

i **Parameter** α: parameter α is the ratio of final tangent stiffness to the initial stiffness, hence, it will be between 0 and 1 (i.e., $0 < \alpha = \frac{k_f}{k} < 1$).

ii **Parameters** β **and** γ: for the Bouc–Wen model to be physically meaningful (the Bounded-Input–Bounded-Output property) and to have the absorbency of input energy and passive performance (not to produce energy), the shape-controlling parameters β and γ should comply with $\beta+\gamma > 0$, $\beta-\gamma \ge 0$, and $\beta \ge 0$ [2,78] which result in $-\beta < \gamma \le \beta$. Then, by conservatively taking $\upsilon = n = 1$ in Eq. (7), it comes to $0 < \beta < \frac{1}{2z_u}$ where z_u can be approximately found as $\max\left(\left|z_{ne} = \frac{F_{ne}-\alpha_1 k u_{ne}}{k(1-\alpha_1)}\right|\right)$ for $ne = 1 \sim N_E$, where z_{ne} is the discrete hysteretic value calculated for N_E experimental data, and α_1 is the ratio of the final tangent stiffness of the first loading path to the initial stiffness.

iii **Parameter** n: shape-controlling parameter n is inversely related to the curvature of the hysteresis loops. As the n increases, the curvature will be decreased. In particular, for $n = 12$, the hysteretic curves will reflect an elastic–plastic behavior [2]. Therefore, it is considered that $1 \le n \le 12$.

iv **Degrading and pinching parameters** (δ_ν, δ_η, q, ζ_s, p, ψ, δ_ψ, **and** λ): because the steel shear walls show hysteretic behavior similar to those for nailed wood joints, a reasonable search domain for degrading and pinching parameters are determined based on the parameters' values reported in [3].

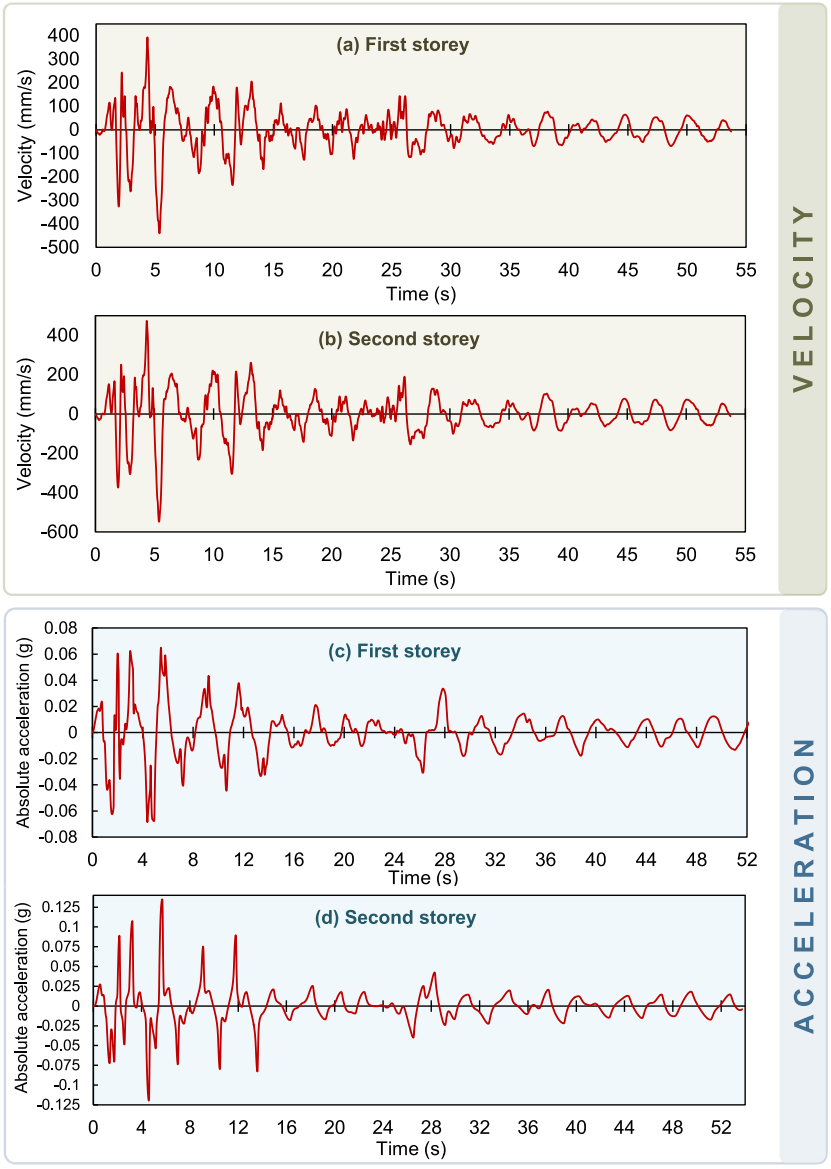

Fig. 12. (**a**) Velocity versus time diagrams for the two stories. (**b**) Absolute acceleration versus time diagrams for the two stories.

Table 3
Side limits for the optimization parameters.

Parameter	α	β	γ	n	δ_v	δ_η	q	ξ_s	p	Ψ	δ_Ψ	λ
Lower bound ($\mathbf{X}_{\min}$)	0.00	0	$-\frac{1}{2z_u}$	1	0.00	0.00	0.00	0.00	0.00	0.00	0.00	0.00
Upper bound ($\mathbf{X}_{\max}$)	1.00	$\frac{1}{2z_u} = 5.00$	$\frac{1}{2z_u}$	12	0.50	0.50	1.00	1.00	10.00	10.00	0.50	1.00

5.5. Parameters of F-CSS

Owing to the randomness of the F-CSS, its performance cannot be judged from the results of a single run. Many trials with independent population initializations should be made to obtain a useful conclusion about the performance of the approach. The best, worst, and mean results obtained from 30 trials with different initial points are used to evaluate the performances of F-CSS. To evaluate the effectiveness of the proposed algorithm, the optimum results of F-CSS are also compared with the results of the standard CSS [14] and the Magnetic CSS (MCSS) [65]algorithms. Sensitivity studies indicate that a population size $N_{cp} = 50$ is sufficient for these problems. The size of the Charged Memory (CM) is equal to N_{cp}. In addition, the maximum number of iterations is set to 500 for the examples. The effect of the previous velocity and resultant force affecting a CP can be controlled by the values of k_v and k_a, respectively. Excessive search in early iterations may improve the exploration ability, however, it must be decreased gradually to increase the exploitation ability. Since k_a is the parameter related to the attracting forces, it works as a control parameter of the exploitation property [50]. Therefore, choosing a linear incremental function (from 1 at the beginning to 1.5 at the end) can improve the performance of the algorithm. Also, the direction of the previous velocity of a CP is not necessarily the same as the resultant force. This shows that velocity coefficient k_v controls the exploration process and therefore a linearly decreasing function (from 2 in the beginning to 0.5 in the end) is selected.

Table 4
Optimal parameters for Specimens A and B.

Parameters (X)		α	β	γ	n	δ_v	δ_η	q	ξ_s	p	Ψ	δ_Ψ	λ
Optimal values	Specimen *A*	0.0814	0.346	−0.279	1.00	0.0	0.0	0.0869	0.959	0.396	0.364	0.002	0.0698
	Specimen *B*	0.0599	0.499	−0.450	1.15	0.0	0.0	0.0754	0.936	0.110	0.574	0.0038	0.4372

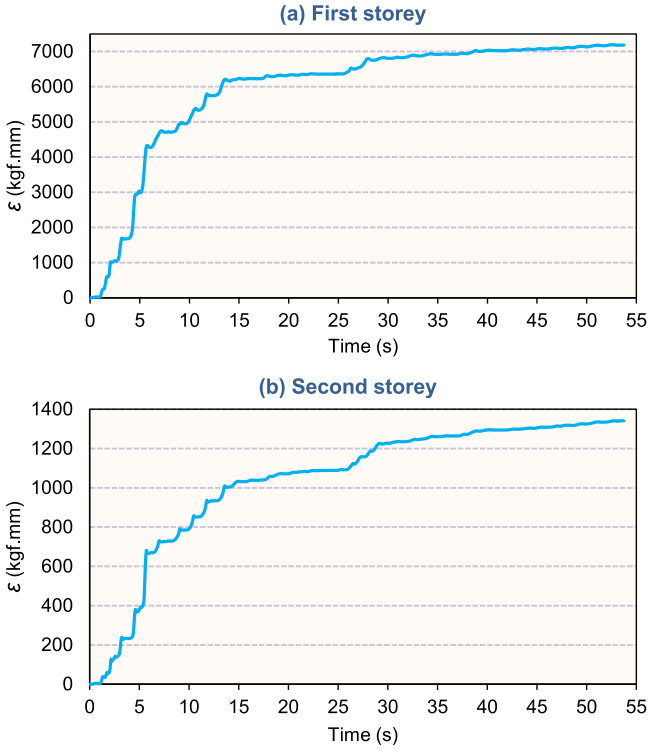

Fig. 13. Hysteretic dissipated energy time histories for (**a**) the first storey, and (**b**) the second storey.

6. Numerical results

6.1. F-CSS simulation results

The F-CSS optimization approach is employed to find the optimum solution for the BWBN model's parameters to lead the model's response to conform to the experimental response. The obtained best optimal parameters' values for specimens A and B with the respective initial stiffness of 809.59 and 982.56 kg/mm are listed in Table 4. The NMSE value of the obtained solutions for specimens A and B are 0.0571 and 0.0589, respectively, which implies that the F-CSS method can convincingly address the parametric identification issue. From the experimental force–displacement curves for the steel shear walls illustrated in Fig. 2b and c, it can be seen that the steel shear panels exhibit non-degrading hysteretic behaviors (i.e., no stiffness and strength degradations). Therefore, the strength and stiffness degrading parameters (i.e., δ_v and δ_η) should become zero, and the number of unknown parameters is decreased to ten. Nevertheless, all twelve parameters were considered in the identification problem in this study to demonstrate a complete procedure applicable to any other lateral-resistant structural systems. As can be seen from Table 4, the obtained values of δ_v and δ_η became zero which validates the BWBN model's parameters and the employed F-CSS optimization scenario.

Fig. 8 illustrates the comparison between the experimental restoring force time-histories of specimens A and B with the BWBN model's predicted response. As can be seen from this figure, the BWBN model's response appropriately recreates the hysteretic restoring force of the steel shear wall subjects. In addition, the comparative force–displacement curves of the experimental and numerical procedures for specimens A and B are presented in Fig. 9a and b, respectively.

To perform a valid comparative study, MCSS, which is a recently-proposed improved version of CSS, is also considered. Table 5 provides the statistical information for these examples obtained using the F-CSS, MCSS, and CSS methods, based on 30 independent runs for each algorithm. The number of required iterations and the population size for all algorithms are considered 500 and 50, respectively. Therefore, the required time for all three algorithms is approximately the same. The superiority of the F-CSS algorithm in terms of the best and average results, as well as standard deviation values, is obvious when the F-CSS's results are compared against the results of the MCSS and CSS algorithms. On a 6 Core™ 2.8 GHz CPU, the required optimization time for the F-CSS algorithm is almost 1198 min, while for the MCSS and CSS algorithms, the times are 1325 and 1250 min, respectively. Table 5 shows that although the differences between the required times are small (2%), in terms of NMSE, the obtained solutions using F-CSS are significantly superior to those obtained using the MCSS and CSS algorithms, respectively.

It should be mentioned that such an optimization process will enable structural designers gain clearer perspective in a preliminary study. To this end, the main aim of this study is to avoid excessive complexities in the design process and achieve some initial estimations using metaheuristics. Importantly, changing the initial conditions of the shear walls will affect the final results; however, the proposed algorithm does not need any additional controls or modifications to be used for the new conditions.

6.2. Numerical structural simulation

A two-degree-of-freedom steel shear wall building example is assumed in which the obtained BWBN hysteretic model's parameters for Specimens A and B (Table 4) characterize the second and first stories' restoring properties, respectively (see Fig. 10a). This case study is considered as a lumped-mass shear building for which the first and second stories' scaled lumped masses are taken as 20 and 8 kg, respectively. A 2% damping ratio ξ for the first two vibrational modes is considered to account for damping mechanisms that the structure would experience during vibrations and Rayleigh's damping matrix [79] is accordingly constructed.

The nonlinear dynamic analysis, as well as the simulation, are conducted in MATLAB and the building responses are analyzed for the 1940 El Centro's earthquake North–South record, as shown in Fig. 10b. The stopping criteria for response tolerances in each iteration are considered as $E_s = 10^{-14}\{\mathrm{S}\}_{i+1}^{P}$ and $E_z = 10^{-14}\{\mathrm{Z}\}_{i+1}^{P}$. The total and maximum step convergence times for the hysteretic analysis of the given case study are illustrated in Fig. 10c as an indication of the computational effort. It reveals that the convergence time for each time step is approximately 0.05 s and the total analysis time is 132 s.

Fig. 10e and f indicate the system's hysteresis behavior in response to seismic excitations by plotting the inter-story drift along the horizontal axis versus hysteretic displacement along the vertical axis. It is observed that the proposed nonlinear dynamic analysis approach can successfully calculate hysteretic displacement and hysteretic restoring force demands for different stories with various hysteretic characteristics to subsequently find the true state of the MDOF structural systems.

Table 5
Performance comparison of the results of F-CSS, MCSS, and CSS.

Performance metric	CSS		MCSS		F-CSS	
	Specimen A	Specimen B	Specimen A	Specimen B	Specimen A	Specimen B
Best result	0.1776	0.2232	0.1663	0.1969	0.0571	0.0589
Average result	0.2532	0.3011	0.2345	0.2822	0.1566	0.1824
Standard deviations	0.1312	0.1722	0.1036	0.1103	0.0756	0.0866
No. of function evaluations	50 × 500 = 25,000		50 × 500 = 25,000		50 × 500 = 25,000	
Optimization time (min.)	1,250		1,325		1,198	

Fig. 11, Fig. 12a & b, and Fig. 12c & d depict the calculated drift, velocity, and absolute acceleration responses of the stories, respectively. The building dissipates the input energy of the earthquake by exhibiting large deformations and ductile performance. The excessive cycles of seismic loading are converted to a finite number of displacement cycles in the structure.

Fig. 13 illustrates the hysteretic energy absorption of the building stories. It can be seen that the dissipated energy diagram is ascending for both stories and the first story absorbs considerably more input energy as it shows far larger drifts compared to the second story. The estimated hysteretic energy dissipation of such structures can be efficiently employed in quantitative loss estimation studies and assessment of cyclic sustainability, failure, and downtime of the structural systems.

7. Conclusions

In this study, a two-stage method for the hysteretic nonlinear analysis of structures based on structural elements' hysteretic demeanors was developed. The proposed approach could be potentially used for the hysteretic analysis of all structural systems which symmetrically resist lateral excitations, and can be further verified through future experimental investigations.

In the first stage, namely system identification, two simply-supported steel shear panels were experimentally studied under cyclic excitations and the BWBN model was utilized to model their experimental hysteretic behavior. It was demonstrated that this model can be employed to portray the hysteretic behavior of structural components with strength degradation, stiffness degradation, and pinching demeanor involved in their cyclic response. A parametric identification of the BWBN model was achieved using the F-CSS metaheuristic optimization method to optimally fit the model's response to experimental results.

In the second stage, a numerical nonlinear analysis method was utilized for the time-history dynamic analysis of MDOF structures using the BWBN hysteretic constitution, where the required computer programming instructions were developed. This approach was used for the analytical simulation of a two-story shear wall building example characterized by the BWBN hysteretic model obtained from the previous stage. The obtained results showed that the proposed analysis approach appropriately incorporated the hysteretic restoring force of structural systems into the nonlinear analysis of structures subjected to arbitrary cyclic-type loadings. This can enable structural designers to calculate the accurate vibrational response and energy absorbability of various structural systems.

The experimental investigation of the BWBN model used in the hysteretic behavior study of the structural components under diverse excitations can be the subject of future research. Besides, developing a new configuration of the BWBN model for the simulation of structural elements with asymmetric hysteresis such as buckling steel braces could be insightful research work. An analytical study of the BWBN model's parameters is also proposed as a future direction to explore the exact physical concepts behind each parameter; and finally, experimental verification of the presented hysteretic analysis results for various MDOF systems is suggested.

It should be noted that the hysteresis model parameters are highly dependent on the utilized loading protocol. In other words, the results of the optimization process and the experimental investigations can be similarly affected by changing the loading protocol. However, the optimization procedure in this study was conducted with the same loading protocol as in the experimental investigations. It is also noteworthy that, given that experimental investigations are generally costly and time-consuming, the proposed F-CSS algorithm can be useful in the preliminary analyses of hysteretic models in structural systems. As future challenges, the applicability of the proposed optimization procedure can be investigated by utilizing different structural systems with different levels of complexity.

Declaration of competing interest

The authors declare that they have no known competing financial interests or personal relationships that could have appeared to influence the work reported in this paper.

Data availability

Data will be made available on request.

References

[1] C.H. Loh, R.C. Ho, Seismic damage assessment based on different hysteretic rules, Earthq. Eng. Struct. Dyn. 19 (5) (1990) 753–771.
[2] G.C. Foliente, Stochastic Dynamic Response of Wood Structural Systems, Virginia Polytechnic Institute and State University, 1993.
[3] G.C. Foliente, Hysteresis modeling of wood joints and structural systems, J. Struct. Eng. 121 (6) (1995) 1013–1022.
[4] H. Zhang, G.C. Foliente, Y. Yang, F. Ma, Parameter identification of inelastic structures under dynamic loads, Earthq. Eng. Struct. Dyn. 31 (5) (2002) 1113–1130.
[5] F. Ma, H. Zhang, A. Bockstedte, G.C. Foliente, P. Paevere, Parameter analysis of the differential model of hysteresis, J. Appl. Mech. 71 (3) (2004) 342–349.
[6] Y. Suzuki, D.G. Lignos, Fiber-based hysteretic model for simulating strength and stiffness deterioration of steel hollow structural section columns under cyclic loading, Earthq. Eng. Struct. Dyn. 49 (15) (2020) 1702–1720.
[7] H. El Jisr, A. Elkady, D.G. Lignos, Hysteretic behavior of moment-resisting frames considering slab restraint and framing action, J. Struct. Eng. 146 (ARTICLE) (2020) 04020145.
[8] S. Kolwankar, A. Kanvinde, M. Kenawy, D. Lignos, S. Kunnath, Simulating cyclic local buckling–induced softening in steel beam–columns using a nonlocal material model in displacement-based fiber elements, J. Struct. Eng. 146 (1) (2020) 04019174.
[9] H. Inamasu, D. Lignos, A. Kanvinde, Effect of column base flexibility on the hysteretic response of wide flange steel columns, in: 3rd Huixian International Forum on Earthquake Engineering for Young Researchers, (CONF) 2017.
[10] Z. Li, F. Albermani, R.W. Chan, S. Kitipornchai, Pinching hysteretic response of yielding shear panel device, Eng. Struct. 33 (3) (2011) 993–1000.
[11] H. Veladi, Study on the Ductility of Steel Shear Walls Ph.D. University of Tabriz, 2011.
[12] S. Talatahari, M. Azizi, M. Toloo, M. Baghalzadeh Shishehgarkhaneh, Optimization of large-scale frame structures using fuzzy adaptive quantum inspired charged system search, Int. J. Steel Struct. 22 (3) (2022) 686–707.

[13] S. Talatahari, M. Azizi, M. Toloo, Fuzzy adaptive charged system search for global optimization, Appl. Soft Comput. 109 (2021) 107518.

[14] A. Kaveh, S. Talatahari, A novel heuristic optimization method: charged system search, Acta Mech. 213 (3) (2010) 267–289.

[15] M. Azizi, S. Talatahari, N. Khodadadi, P. Sareh, Multiobjective atomic orbital search (MOAOS) for global and engineering design optimization, IEEE Access 10 (2022) 67727–67746.

[16] S. Talatahari, M. Azizi, M. Tolouei, B. Talatahari, P. Sareh, Crystal structure algorithm (CryStAl): a metaheuristic optimization method, IEEE Access 9 (2021) 71244–71261.

[17] H.T. Sadeeq, A.M. Abdulazeez, Giant trevally optimizer (GTO): A novel metaheuristic algorithm for global optimization and challenging engineering problems, IEEE Access (2022).

[18] E. Bogar, S. Beyhan, Adolescent identity search algorithm (AISA): A novel metaheuristic approach for solving optimization problems, Appl. Soft Comput. 95 (2020) 106503.

[19] O.N. Oyelade, A.E.-S. Ezugwu, T.I. Mohamed, L. Abualigah, Ebola optimization search algorithm: A new nature-inspired metaheuristic optimization algorithm, IEEE Access 10 (2022) 16150–16177.

[20] Y.-H. Chou, S.-Y. Kuo, L.-S. Yang, C.-Y. Yang, Next generation metaheuristic: jaguar algorithm, IEEE Access 6 (2018) 9975–9990.

[21] J.-S. Chou, D.-N. Truong, A novel metaheuristic optimizer inspired by behavior of Jellyfish in ocean, Appl. Math. Comput. 389 (2021) 125535.

[22] P. Savsani, V. Savsani, Passing vehicle search (PVS): A novel metaheuristic algorithm, Appl. Math. Model. 40 (3951) (2016) 5-6–3978.

[23] F. Zitouni, S. Harous, R. Maamri, The solar system algorithm: a novel metaheuristic method for global optimization, IEEE Access 9 (2020) 4542–4565.

[24] N. Khodadadi, M. Azizi, S. Talatahari, P. Sareh, Multi-objective crystal structure algorithm (MOCryStAl): introduction and performance evaluation, IEEE Access 9 (2021) 117795–117812.

[25] M. Dorigo, T. Stützle, The ant colony optimization metaheuristic: algorithms, applications, and advances, in: Handbook of Metaheuristics, 2003, pp. 250–285.

[26] X.-S. Yang, Nature-Inspired Metaheuristic Algorithms, Luniver Press, 2010.

[27] T. Dokeroglu, E. Sevinc, T. Kucukyilmaz, A. Cosar, A survey on new generation metaheuristic algorithms, Comput. Ind. Eng. 137 (2019) 106040.

[28] V. Goodarzimehr, S. Talatahari, S. Shojaee, S. Hamzehei-Javaran, P. Sareh, Structural design with dynamic constraints using weighted chaos game optimization, J. Comput. Des. Eng. 9 (6) (2022) 2271–2296.

[29] B. Talatahari, M. Azizi, S. Talatahari, M. Tolouei, P. Sareh, Crystal structure optimization approach to problem solving in mechanical engineering design, Multidiscip. Model. Mater. Struct. (2022).

[30] P. Sareh, The least symmetric crystallographic derivative of the developable double corrugation surface: Computational design using underlying conic and cubic curves, Mater. Des. 183 (2019) 108128.

[31] Y. Chen, J. Yan, J. Feng, P. Sareh, A hybrid symmetry–PSO approach to finding the self-equilibrium configurations of prestressable pin-jointed assemblies, Acta Mech. 231 (4) (2020) 1485–1501.

[32] Y. Chen, C. Lu, J. Yan, J. Feng, P. Sareh, Intelligent computational design of scalene-faceted flat-foldable tessellations, J. Comput. Des. Eng. 9 (5) (2022) 1765–1774.

[33] P. Sareh, S.D. Guest, Design of non-isomorphic symmetric descendants of the Miura-ori, Smart Mater. Struct. 24 (8) (2015) 085002.

[34] P. Sareh, S.D. Guest, Designing symmetric derivatives of the Miura-ori, in: Advances in Architectural Geometry 2014, Springer, 2015, pp. 233–241.

[35] M. Azizi, S. Talatahari, P. Sareh, Design optimization of fuzzy controllers in building structures using the crystal structure algorithm (CryStAl), Adv. Eng. Inform. 52 (2022) 101616.

[36] H. Sadeeq, A. Abdulazeez, N. Kako, A. Abrahim, A novel hybrid bird mating optimizer with differential evolution for engineering design optimization problems, in: International Conference of Reliable Information and Communication Technology, Springer, 2017, pp. 522–534.

[37] P. Sareh, Symmetric Descendants of the Miura-Ori Ph.D, Department of Engineering University of Cambridge, 2014.

[38] P. Sareh, Y. Chen, Intrinsic non-flat-foldability of two-tile DDC surfaces composed of glide-reflected irregular quadrilaterals, Int. J. Mech. Sci. 185 (2020) 105881.

[39] Q. Hua, J. He-fu, W. Wei-dong, W. Chang-bo, Design of a turbine blade with multidisciplinary design optimization (MDO) method, Multidiscip. Model. Mater. Struct. (2006).

[40] P. Sareh, S.D. Guest, Design of isomorphic symmetric descendants of the Miura-ori, Smart Mater. Struct. 24 (8) (2015) 085001.

[41] Y. Chen, J. Yan, J. Feng, P. Sareh, Particle swarm optimization-based metaheuristic design generation of non-trivial flat-foldable origami tessellations with degree-4 vertices, J. Mech. Des. 143 (1) (2021).

[42] S. Talatahari, M. Azizi, Chaos game optimization: a novel metaheuristic algorithm, Artif. Intell. Rev. 54 (2) (2021) 917–1004.

[43] S. Talatahari, M. Azizi, Optimization of constrained mathematical and engineering design problems using chaos game optimization, Comput. Ind. Eng. 145 (2020) 106560.

[44] S. Talatahari, M. Azizi, Optimum design of building structures using tribe-interior search algorithm, in: Structures, Vol. 28, Elsevier, 2020, pp. 1616–1633.

[45] V. Goodarzimehr, S. Talatahari, S. Shojaee, S. Hamzehei-Javaran, Special relativity search for applied mechanics and engineering, Comput. Methods Appl. Mech. Engrg. 403 (2023) 115734.

[46] A. Greco, A. Pluchino, F. Cannizzaro, An improved ant colony optimization algorithm and its applications to limit analysis of frame structures, Eng. Optim. (2019).

[47] S. Talatahari, M. Azizi, Optimal design of real-size building structures using quantum-behaved developed swarm optimizer, Struct. Des. Tall Special Build. 29 (11) (2020) e1747.

[48] S. Talatahari, P. Motamedi, B. Farahmand Azar, M. Azizi, Tribe–charged system search for parameter configuration of nonlinear systems with large search domains, Eng. Optim. 53 (1) (2021) 18–31.

[49] S. Talatahari, A. Kaveh, R. Sheikholeslami, Engineering design optimization using chaotic enhanced charged system search algorithms, Acta Mech. 223 (10) (2012) 2269–2285.

[50] A. Kaveh, S. Talatahari, Hybrid charged system search and particle swarm optimization for engineering design problems, Eng. Comput. 28 (4) (2011) 423–440.

[51] M. Azizi, R.G. Ejlali, S.A.M. Ghasemi, S. Talatahari, Upgraded whale optimization algorithm for fuzzy logic based vibration control of nonlinear steel structure, Eng. Struct. 192 (2019) 53–70.

[52] B. Nouhi, N. Darabi, P. Sareh, H. Bayazidi, F. Darabi, S. Talatahari, The fusion–fission optimization (FuFiO) algorithm, Sci. Rep. 12 (1) (2022) 1–44.

[53] M. Azizi, S. Talatahari, M. Basiri, M.B. Shishehgarkhaneh, Optimal design of low-and high-rise building structures by Tribe-Harmony search algorithm, Decis. Anal. J. (2022) 100067.

[54] B. Nouhi, Y. Jahani, S. Talatahari, A. Gandomi, A swarm optimizer with modified feasible-based mechanism for optimum structure in steel industry, Decis. Anal. J. 5 (2022) 100129.

[55] K.M. Ong, P. Ong, C.K. Sia, A new flower pollination algorithm with improved convergence and its application to engineering optimization, Decis. Anal. J. (2022) 100144.

[56] U. Dereci, M.E. Karabekmez, The applications of multiple route optimization heuristics and meta-heuristic algorithms to solid waste transportation: A case study in Turkey, Decis. Anal. J. 4 (2022) 100113.

[57] P. Chakraborty, S. Nama, A.K. Saha, A hybrid slime mould algorithm for global optimization, Multimedia Tools Appl. (2022) 1–27.

[58] S. Nama, A.K. Saha, S. Ghosh, Improved backtracking search algorithm for pseudo dynamic active earth pressure on retaining wall supporting c-Φ backfill, Appl. Soft Comput. 52 (2017) 885–897.

[59] S. Chakraborty, A.K. Saha, S. Sharma, S. Mirjalili, R. Chakraborty, A novel enhanced whale optimization algorithm for global optimization, Comput. Ind. Eng. 153 (2021) 107086.

[60] A.S. Eesa, Z. Orman, A.M.A. Brifcani, A novel feature-selection approach based on the cuttlefish optimization algorithm for intrusion detection systems, Expert Syst. Appl. 42 (5) (2015) 2670–2679.

[61] A. Chakri, R. Khelif, M. Benouaret, Improved bat algorithm for structural reliability assessment: application and challenges, Multidiscip. Model. Mater. Struct. (2016).

[62] T. Ting, X.-S. Yang, S. Cheng, K. Huang, Hybrid metaheuristic algorithms: past, present, and future, in: Recent Advances in Swarm Intelligence and Evolutionary Computation, 2015, pp. 71–83.

[63] B. Morales-Castañeda, D. Zaldivar, E. Cuevas, F. Fausto, A. Rodríguez, A better balance in metaheuristic algorithms: Does it exist? Swarm Evol. Comput. 54 (2020) 100671.

[64] S. Talatahari, A. Kaveh, N. Mohajer Rahbari, Parameter identification of Bouc-Wen model for MR fluid dampers using adaptive charged system search optimization, J. Mech. Sci. Technol. 26 (8) (2012) 2523–2534.

[65] S. Talatahari, J. Faramarzi, Optimum grillage systems design using magnetic charged system search algorithm, Iran. J. Struct. Eng. 4 (2) (2017) 108–114.

[66] R. Parsiavash, M.T. Alami, S. Talatahari, A hybrid magnetic CSS and BBBC for optimum design of double curvature arch dams, Jordan J. Civ. Eng. 11 (2) (2017).

[67] R. Bouc, Forced vibrations of mechanical systems with hysteresis, in: Proc. of the Fourth Conference on Nonlinear Oscillations, Prague, 1967, 1967.

[68] Y.-K. Wen, Method for random vibration of hysteretic systems, J. Eng. Mech. Div. 102 (2) (1976) 249–263.

[69] T.T. Baber, Y.-K. Wen, Random vibration of hysteretic, degrading systems, J. Eng. Mech. Div. 107 (6) (1981) 1069–1087.

[70] T.T. Baber, M.N. Noori, Random vibration of degrading, pinching systems, J. Eng. Mech. 111 (8) (1985) 1010–1026.

[71] A. Charalampakis, V. Koumousis, Identification of Bouc–Wen hysteretic systems by a hybrid evolutionary algorithm, J. Sound Vib. 314 (3–5) (2008) 571–585.

[72] A. Charalampakis, C. Dimou, Identification of Bouc–Wen hysteretic systems using particle swarm optimization, Comput. Struct. 88 (1197) (2010) 21-22–1205.

[73] Y. Ni, J. Ko, C. Wong, Identification of non-linear hysteretic isolators from periodic vibration tests, J. Sound Vib. 217 (4) (1998) 737–756.

[74] C. Crivellaro, S.J. Alves, Phenomenological Model of a Magneto-Rheological Damper for Semi-Active Suspension Control Design and Simulation, SAE Technical Paper, 2006, pp. 0148–7191.

[75] F. Raeesi, B.F. Azar, H. Veladi, S. Talatahari, An inverse TSK model of MR damper for vibration control of nonlinear structures using an improved grasshopper optimization algorithm, in: Structures, Vol. 26, Elsevier, 2020, pp. 406–416.
[76] X. Zhu, X. Lu, Parametric identification of Bouc-Wen model and its application in mild steel damper modeling, Procedia Eng. 14 (2011) 318–324.
[77] S.-S. Lin, J.-C. Liao, T.-T. Liang, C. Juang, Use of Bouc-Wen model for seismic analysis of concrete piles, in: Deep Foundations 2002: An International Perspective on Theory, Design, Construction, and Performance, 2002, pp. 372–384.
[78] M. Ismail, F. Ikhouane, J. Rodellar, The hysteresis Bouc-Wen model, A survey, Arch. Comput. Methods Eng. 16 (2) (2009) 161–188.
[79] A.K. Chopra, Theory and applications to earthquake engineering, Dyn. Struct. (1995).
[80] N. Mohajer Rahbari, B. Farahmand Azar, S. Talatahari, H. Safari, Semi-active direct control method for seismic alleviation of structures using MR dampers, Struct. Control Health Monit. 20 (6) (2013) 1021–1042.
[81] A. Bahar, F. Pozo, L. Acho, J. Rodellar, A. Barbat, Hierarchical semi-active control of base-isolated structures using a new inverse model of magnetorheological dampers, Comput. Struct. 88 (7–8) (2010) 483–496.